CRYSTAL GROWTH & DESIGN

Article

pubs.acs.org/crystal

Selective Epitaxial Growth on Germanium Nanowires via Hybrid Oxide-Stabilized/Vapor–Liquid–Solid Growth

Christopher J. Hawley, Terrence McGuckin, and Jonathan E. Spanier*

Department of Materials Science & Engineering, Drexel University, Philadelphia, Pennsylvania 19104, United States

Supporting Information

ABSTRACT: The introduction low levels of oxygen during the vapor–liquid–solid growth (VLS) of germanium nanowires causes an oxide sheath to form at the catalyst/nanowire/vapor interface during growth. This results in extremely high aspect ratio nanowires due to the removal of homoepitaxial deposition and the finite energy required for heterogeneous nucleation of germanium on its oxide. With the removal of oxygen, the catalyzed oxide sheath terminates and conventional growth with finite sidewall deposition dominates subsequent growth. The successful transition between oxide-stabilized and conventional VLS regimes can be deliberately manipulated to grow finite conical nanowire segments with discontinuous changes in diameter.

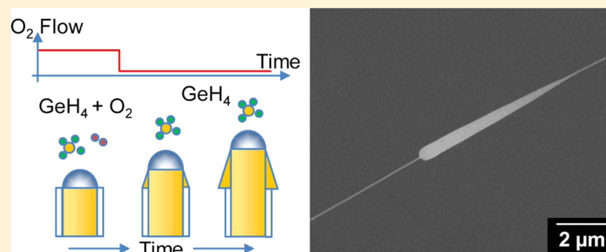

The *ab initio* design and synthesis of nanoscale semiconductor building blocks is key in realizing bottom-up routes for nanowire-based science and technology. Advances in hierarchical nanowire (NW) synthesis have enabled tailoring of composition[1,2] and doping,[3] both axially[4−10] and radially,[6,11−28] permitting the study of finite-size effects and phenomena owing to the high-aspect ratio of these quasi one-dimensional nanostructures. The tailorability of NW segments is of fundamental interest to the field of NW synthesis and their technological integration. We propose that the directed radial growth of specifically controlled NW segments, where the core NW axial segments are distinguished by different surface composition, represents a new method of controlling NW morphology via precursor incorporation. The tailorable diameter of these NWs provides new opportunities for the access of and control over electrical, optical, and magnetic finite-size effects. Significantly, this growth mechanism can be utilized to introduce selective surface passivation *in situ* to promote or suppress the adsorption of a precursor species with implications for multiprecursor synthesis where both catalyst adsorption and sidewall deposition are tailorable parameters.

Outstanding challenges in existing bottom-up device fabrication indicate a need for the highly controllable design of NW morphology as an alternative to postgrowth processing techniques employed to alter NW morphology, processes which add additional steps and can be difficult to control. Typical in vapor–liquid–solid (VLS) NW growth is a tapering of diameter as precursor deposition occurs at a continuous rate on the sidewall of a NW (Figure 1a).[6,20,22,25,26] Surface diffusion of gold in VLS growths[17,24] also produces tapering as catalyst atoms diffuse between NW tips. However these processes only allow tapering due to gold catalyst loss and are solely a VLS mechanism with no ability to produce radial discontinuities nor the potential to change precursor chemisty. Commonly, oxide incorporation is used to tailor morphologies.[15,21−23,29,30] A primary method for incorporating oxygen is the NW growth mechanism of oxide assisted growth[31,32] (OAG) which is used as a catalyst free, non-VLS growth method. The OAG mechanism, beyond nucleating and growing NWs, benefits from a thin oxide layer on the outside of the NW. This oxide successfully stabilizes the NW surface and prohibits the successful adsorption of precursor species on the sidewall, leading to little or no tapering over the length of the NW (Figure 1b).

Here, we demonstrate the *in situ* selective formation of Ge and GeO_x NW surfaces using the transition between the OAG regime[8,17,18,31] and conventional VLS growth. By manipulating the transition between the two growth regimes through the use of passivated surfaces midgrowth, we obtain segmented radial discontinuities during NW growth. These segments can vary in both length and aspect ratio, depending on the conditions, and form a diameter discontinuity at the position along the wire where oxide incorporation begins. We present a bottom-up growth method with new implications for selective NW core–shell adsorption where the use of passivated surfaces can be employed midgrowth to manipulate specific locations for species deposition. The process can be tailored to produce a variety of radial discontinuities as well as segment lengths to suit a wide variety of finite size optical, electronic and magnetic applications.

METHODS

Sample Preparation. Solvents and DI water, followed by oxygen plasma cleaning, are used to clean oxidized Si(100) wafers. The substrates are then submerged in poly L-lysine (Ted Pella) for 2 min, rinsed in DI water, dried and then submerged in 40 nm gold colloid solution (Ted Pella) for 5 min, rinsed and dried. Another plasma

Received: May 31, 2012

ACS Publications © XXXX American Chemical Society

dx.doi.org/10.1021/cg3016595 | Cryst. Growth Des. XXXX, XXX, XXX−XXX

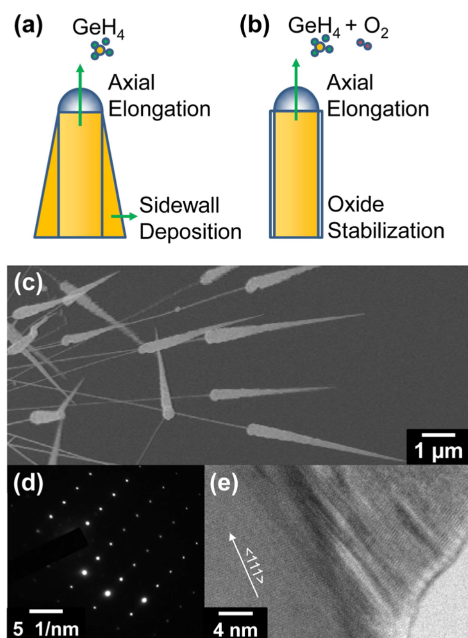

Figure 1. (a) A comparison between typical CVD grown NWs and (b) oxide-stabilized NW growth. In CVD, both axial and radial growth rates are finite, leading to NW tapering. Consistent with OAG, an oxide is used to stabilize the diameter of NWs during growth to eliminate significant sidewall deposition. (c) Demonstration of the transition from oxide-stabilized to conventional tapered CVD growth. (d) SAED showing the ⟨111⟩ growth direction which is confirmed with HRTEM. (e) Also seen in the HRTEM are the lattice planes of the nucleated grain which transition to their new orientation over 5 nm.

cleaning is used to remove residue from this process. These substrates are placed in the center of a chemical vapor deposition (CVD) tube furnace reactor where 3.5 to 7 Torr partial pressure germane (10% by volume GeH_4/H_2, Voltaix) in hydrogen (Airgas) is used at 70 Torr and 375 °C. We find that the conditions which induce an abrupt transition between tapered and solely axial growth, resulting in a maximum difference in NW radius, correlate with a higher temperature and higher partial pressure than our optimized standard VLS NW growth. To introduce oxygen flow, we create a custom mix of oxygen and nitrogen (Airgas) to introduce with the germane at 1 sccm. A 10% oxygen content transitions between growth regimes for our growth reactor and given conditions. Special attention is given to oxygen levels early in the growth process where catalyst nucleation and poisoning are issues of concern.

Characterization. The Ge postgrowth oxide-stabilized NW morphology was imaged with field-emission scanning electron microscopy (SEM, FEI DB235 and Amray 1850). Selected area electron diffraction (SAED) and energy-dispersive X-ray spectra (EDS) were taken using a JEOL JEM2100 LaB_6 transmission electron microscope (TEM) at a 200 kV accelerating voltage.

■ RESULTS AND DISCUSSION

We first demonstrate the synthesis of Ge NWs with an abrupt transition between the oxide-stabilized and conventional VLS growth regimes. The synthesized wires have diameters consistent with the 40 nm catalyst size and primarily grow in the ⟨111⟩ direction with no change in orientation due to the transition between growth regimes. The robustness of the technique is shown in the transition from oxide-stabilized to oxygen-free growth segments (Figure 2a,b) and vice versa (Figure 2c,d). Three step growths shed light on the surface chemistry based method demonstrated in that the oxide persists in its control of Ge nuclei. The NW surface is not reduced by GeH_4 or H_2, nor do the growths exceed the incubation period for Ge nucleation on its oxide. Not exceeding the incubation period is significant due to the relatively large time scales involved. Incubation times have been shown to have great dependence on the preparation and cleanliness of the surface.[33−35] Freshly grown NWs, with no exposure to atmospheric oxygen partial pressures, water vapor, etc., have surfaces that are extremely clean and can lead to incubation periods exceeding 25 min under the specified experimental conditions. These growths are in stark contrast with diffusion based methods[17] which can only reproduce morphologies akin

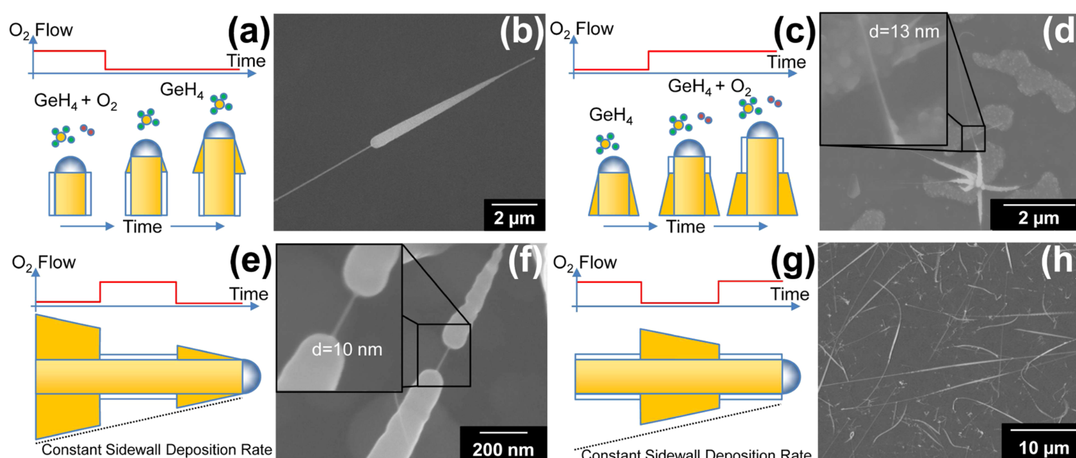

Figure 2. (a, b) During growth, the transition between oxide-stabilized and tapered segments is achieved by reducing the flow of oxygen below a threshold associated with further oxide sidewall incorporation. In our system, this is best achieved by turning 1 sccm of 10% O_2 on and off. (c, d) Lower oxygen levels are needed to nucleate NWs and begin the VLS growth process. By raising the oxygen level, oxide incorporation turns on midgrowth and produces long thin wires from the initial seed. Note that sidewall deposition continues on the seed in this case. (e, f) By changing the oxygen flow rate during growth, a successful transition between tapered sections and oxide-stabilized sections can be achieved. The continuation of sidewall deposition in the region of initial growth is evidence of catalyst involvement in the oxide formation. (g, h) By reducing the flow of oxygen during the NW growth, segments of larger diameter can be created. The limits of these changes lie in the growth conditions of temperature, pressure, etc., but can also be enhanced by increasing the growth time.

to Figure 1c. In addition, order of magnitude quasi-discontinuities can be achieved, far greater than solely VLS based catalyst wetting morphological control[16] which neglects the potential utilization of the NW surface chemistry. We are able to confirm the polycrystalline nature of the shell structures via TEM showing grains growing from the ⟨111⟩ oriented core (Figure 1d,e). The conical segments initially grow homoepitaxially, but quickly transition to polycrystalline due to the high growth rate which results in a higher generation of defects.[36] A thin oxide of a few nanometers is seen in TEM as is typical in Ge growth exposed to atmospheric oxygen and water vapor.

As suggested by an abrupt growth transition, the modulation of multiple segmented growths was subsequently investigated. As is conventional with VLS growth, the significant oxygen presence at the beginning of the growth process can poison catalysts and greatly reduce nucleation of NWs. After producing a tapered nucleation segment, we oxide-stabilize the sidewalls for varying segment lengths, and then return to oxygen-free growth conditions where tapering resumes (Figure 2e,f). Consistent with OAG is that the oxide incorporates into the NW at the catalyst and does not simply oxidize any exposed sidewall; this is evident with previous tapered segments resuming radial growth after an oxide growth step. The oxidation at the catalyst-sidewall interface increases the functionality of this process as the sidewall deposition can continue with the growth and create extremely high radial discontinuities for very short oxide-stabilized segments (Figure 2f).

The inverse of the oxide-stabilized segment in a tapered nanostructure is also investigated to create nanostructures more akin to NWs with radially larger tapered segments (Figure 2g,h). As oxygen flow ceases, the NW begins to incorporate Ge into the sidewalls and tapering occurs. With the reintroduction of oxygen, the catalyzed sidewall oxidation begins again and the NW continues to grow at the same diameter as before. These nanostructures are made to favor the NW morphology with more robust oxide segments and a longer incubation period.[37−39] This is expanded to five segments to demonstrate robustness and, again, the change in radius increases in the earlier grown segments if multiple tapered segments are grown (Figure 3).

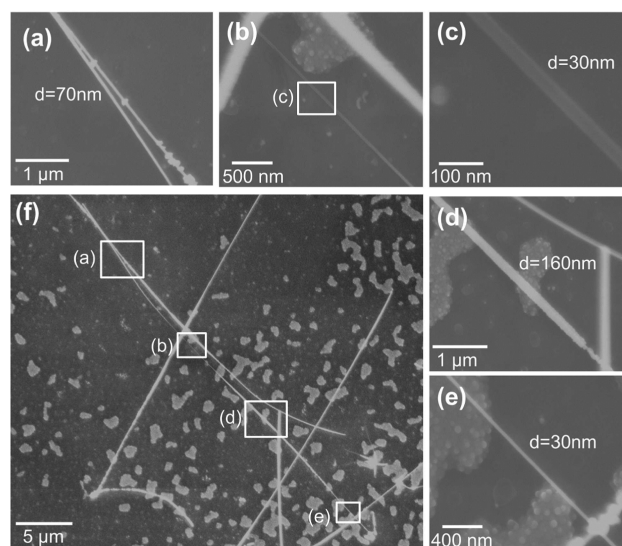

Figure 3. (a−e) As-grown NW where the radial and oxide-stabilized growth are alternated to tailor specific NW segments to have greater diameters than the catalyst dictated core dimension.

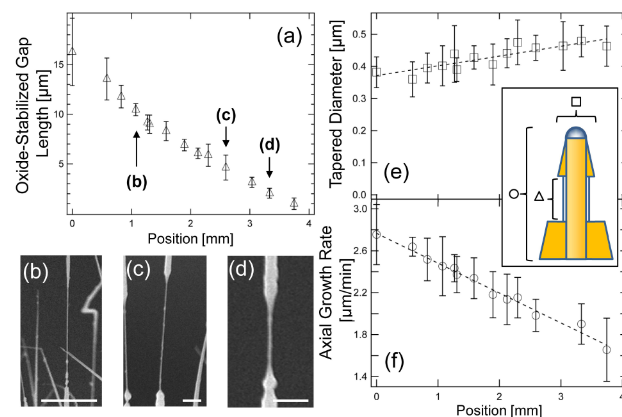

Figure 4. (a) The oxide-stabilized segment gap length vs increasing substrate position from the furnace center with (b−d) examples shown; scale bars are 5 μm, 1 μm, and 1 μm, respectively. The tapered diameter (e) and axial growth rate (f) for the same samples supports the conventional VLS growth in a hot-walled reactor.

The process is performed at a single central furnace position, but the morphology changes dramatically both upstream and downstream from this position, denoted position = 0, as seen in Figure 4. The axial growth rate increases with GeH_4 partial pressure while the tapering decreases with GeH_4 partial pressure and increases with temperature, consistent with previous results,[20,26] and signifying that the growth has a foundation in VLS. The selective deposition is also position dependent, which we quantify here using the physical gap length of the oxide-stabilized region. Analysis from a single growth run shows this quantity changes with position even though the segments are formed using equal oxygen exposure times. We have developed a qualitative reaction model (Appendix A) with input considering our experimental setup which supports the gap length behavior shown in Figure 4.

The existence of an incubation period defines $k_{-1} > k_2$ in the tailorable growth region,[40] where k_{-1} is the desorption of GeH_4 from the NW surface and k_2 involves the precursor decomposition; however, the change in gap length with position demands that these reaction constants not be fixed with position since decreasing GeH_4 partial pressure, increasing H_2 partial pressure, as well as other experimental model components cannot alone account for these results. A supplemental component to the reaction model is surface diffusion,

$$D_s = D_s^o[*]e^{-E_d/kT} \quad (1)$$

which increases with free adsorption site density [*], where D_s^o is a constant and E_d is the surface diffusion activation energy.[41] Using experimental considerations, in this case the observable existence of an incubation period, [*] is approximated as

$$[*] \approx \frac{n_o}{1 + K_1 p_{GeH_4} + K_3 p_{H_2}^{1/2}} \quad (2)$$

where n_o is the density of surface sites, K_1 governs the adsorption and desorption of precursor, K_3 governs the adsorption and desorption of hydrogen, and p_{GeH_4} and p_{H_2} define the germane and hydrogen vapor pressures, respectively. This, coupled with the depletion of GeH_4 along the reactor, supports the experimental observations of the decreasing oxide

dx.doi.org/10.1021/cg3016595 | Cryst. Growth Des. XXXX, XXX, XXX−XXX

segment length, and while surface diffusion is very limited on oxide surfaces and is significant here due to the clean surface conditions on the freshly grown wires. The growth reactor increases in temperature with position as is common in practice to combat reduced deposition from the barrier layer. This has the effect of increasing K_2 as well as in the Ge−O system increasing the vapor pressure of GeO(g). Increasing K_2 will lead to higher deposition rates, while the GeO(g) creation will remove the catalyzed oxide sheath and lead to lower incubation periods as the surface transitions to the GeH_4−Ge(s) system. With very little O_2(g) being introduced into the system, the percent change of the O_2 partial pressure will be the greatest of the introduced gases, followed by the GeH_4 and the H_2. The O_2 consumption into GeO_x gaseous and solid compounds is nontrivial. With the considerations of laminar flow and the relatively short length scales involved in analyzing the oxide-stabilized gap length region, we discount the possibility that introduced gas will turbulently mix and that it significantly affects the decreasing gap length with furnace position trend.

The lateral nature of the growths is evident with a clear oxide segment preserved even as the growth conditions change to decrease the gap length. This effect cannot be solely explained with previous considerations of temperature (K_2), GeO(g), or decreasing O_2 partial pressure as these lead to simultaneously enhanced nucleation rates on all grown oxide-stabilized surfaces. Lateral growth has been attributed to partial pressure gradients,[42] but the NW morphology combined with the constantly flowing gas makes this explanation unlikely for this situation. Similar to the case of enhanced incubation times with rigorously cleaned substrates,[33−35] these as-grown wires have been exposed only to the growth reactor and are relatively free of surface contaminants, which enhances the surface diffusion of the species and nontrivially contributes to lateral growth and decreasing oxide gap length.

■ CONCLUSIONS

In summary, we have grown Ge NWs in both the oxide-stabilized diameter regime and the conventional VLS regime, and we demonstrate the transition between the two via a change in oxygen incorporation during the growths. We show different means of using this technique to grow novel nanostructures containing large radial discontinuities with tailorable dimensions and segment lengths. Grown in a conventional CVD reactor, the accessibility and tailorability of this method for bottom-up growth of NW-based structures provides an excellent framework for the study of phonon propagation, incorporation of alloyed materials or dopants, spatial control of photon absorption, or any other finite-size effect seen in Ge on these radial length scales.

■ APPENDIX A

A model giving context to the many interconnective and competitive processes occurring during growth of these nanostructures is considered. This model is based on previous selective surface reaction models by Bloem and Claassen[40,41] and is considered for the reactor geometry of the present experiment as well as for the addition of GeO_x solid and gaseous species.

The process begins with the introduced bulk GeH_4(b) through the diffusion barrier layer toward the growth substrate, where it is then denoted GeH_4(g):

$$\mathrm{GeH_4(b)} \underset{k_{-a}}{\overset{k_a}{\rightleftharpoons}} \mathrm{GeH_4(g)} \tag{3}$$

We then consider adsorption site reactions, where * denotes a free surface site:

$$* + \mathrm{GeH_4(g)} \underset{k_{-1}}{\overset{k_1}{\rightleftharpoons}} \mathrm{GeH_4^*} \tag{4}$$

$$\mathrm{GeH_4^*} \underset{k_{-2}}{\overset{k_2}{\rightleftharpoons}} \mathrm{Ge^*} + 2\mathrm{H_2} \tag{5}$$

$$\frac{1}{2}\mathrm{H_2} + * \underset{k_{-3}}{\overset{k_3}{\rightleftharpoons}} \mathrm{H^*} \tag{6}$$

$$\mathrm{Ge^*} \underset{k_{-4}}{\overset{k_4}{\rightleftharpoons}} \mathrm{Ge(st)} + * \tag{7}$$

$$\mathrm{Ge^*} \underset{k_{-5}}{\overset{k_5}{\rightleftharpoons}} \mathrm{Ge(g)} + * \tag{8}$$

Also necessary for the Ge−O system is the formation of the oxide solid and gaseous species:

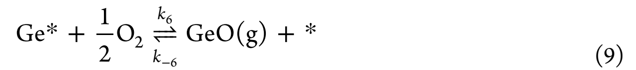

$$\mathrm{Ge^*} + \frac{1}{2}\mathrm{O_2} \underset{k_{-6}}{\overset{k_6}{\rightleftharpoons}} \mathrm{GeO(g)} + * \tag{9}$$

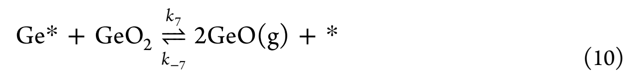

$$\mathrm{Ge^*} + \mathrm{GeO_2} \underset{k_{-7}}{\overset{k_7}{\rightleftharpoons}} 2\mathrm{GeO(g)} + * \tag{10}$$

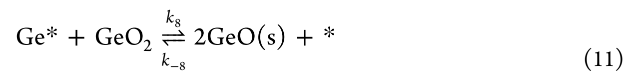

$$\mathrm{Ge^*} + \mathrm{GeO_2} \underset{k_{-8}}{\overset{k_8}{\rightleftharpoons}} 2\mathrm{GeO(s)} + * \tag{11}$$

$$\mathrm{Ge^*} + \mathrm{O_2(g)} \underset{k_{-9}}{\overset{k_9}{\rightleftharpoons}} \mathrm{GeO_2} + * \tag{12}$$

This leads to the free surface site density [*]:

$$[*] = n_0 - [\mathrm{GeH_4^*}] - [\mathrm{Ge^*}] - [\mathrm{H^*}] - \ldots \tag{13}$$

and the adsorbed GeH_4 density:

$$[\mathrm{GeH_4^*}] = \frac{k_1[*]p_{\mathrm{GeH_4}} + k_{-2}[Ge^*]p_{\mathrm{H_2}}^2}{k_{-1} + k_2} \tag{14}$$

We let

$$k_{-1} \gg k_2 \tag{15}$$

as a fundamental requirement for the existence of an incubation time and

$$[\mathrm{GeH_4^*}] \approx K_1 p_{\mathrm{GeH_4}} \tag{16}$$

where K_i is defined as

$$K_i \equiv \frac{k_i}{k_{-i}} \tag{17}$$

$$[\mathrm{Ge^*}] = \frac{k_2[\mathrm{GeH_4^*}] + [*](k_{-6}p_{\mathrm{GeO}} + k_{-7}p_{\mathrm{GeO}}^2 + k_{-8})}{k_4 + k_5 + k_6 p_{\mathrm{O_2}}^{1/2} + k_7 + k_8 + k_9 p_{\mathrm{O_2}} + k_{-2}p_{\mathrm{H_2}}^2} \tag{18}$$

with k_2 kinetically dominant over k_{-7} and k_{-8} as well as pGeH$_4$ ≫ pGeO which gives the qualitative behavior of [Ge*] as well as helps define the growth rate which is proportional to [Ge*]

dx.doi.org/10.1021/cg3016595 | Cryst. Growth Des. XXXX, XXX, XXX−XXX

and dominated by the $k_2[\mathrm{GeH}_4^*]$ term. Similarly, we find the adsorbed hydrogen density:

$$[\mathrm{H}^*] = K_3 p_{\mathrm{H}_2}^{1/2}[*] \quad (19)$$

Combining all these surface terms gives the density of free surface sites:

$$[*] \approx \frac{n_0}{1 + K_1 p_{\mathrm{GeH}_4} + K_3 p_{\mathrm{H}_2}^{1/2}} \quad (20)$$

with $[\mathrm{GeH}_4^*]$ and $[\mathrm{H}^*] \gg [\mathrm{Ge}^*]$ due to the relatively fast kinetics associated with $[\mathrm{Ge}^*]$.

It is important to recognize that this model was developed to include the complexity required to properly consider the dominant processes in growing these nanostructures, but it is by no means meant to exhaustively explore the possible reactions in this system. A subtle, yet important example is the decomposition of GeH_4, where the most probable chain of reactions[43] is

$$\mathrm{GeH_4(g)} \rightleftharpoons \mathrm{GeH}_4^* \quad (21)$$

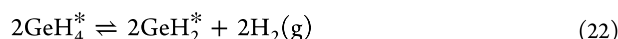

$$2\mathrm{GeH}_4^* \rightleftharpoons 2\mathrm{GeH}_2^* + 2\mathrm{H_2(g)} \quad (22)$$

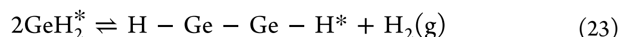

$$2\mathrm{GeH}_2^* \rightleftharpoons \mathrm{H - Ge - Ge - H^*} + \mathrm{H_2(g)} \quad (23)$$

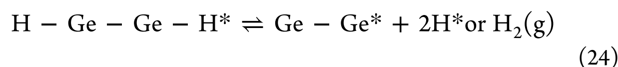

$$\mathrm{H - Ge - Ge - H^*} \rightleftharpoons \mathrm{Ge - Ge^*} + 2\mathrm{H^*} \text{or } \mathrm{H_2(g)} \quad (24)$$

Though the reactions of eqs 21−24 should dominate, in reality all GeH_x species will manifest to some degree. In practice, due to the convoluted nature of these reactions and the resultant adsorbed Ge, we summarize these forward and reverse reactions, between all the Ge−H species, together as an effective rate constant (k_2 and k_{-2}). Similarly, negligibly small species, such as H_2O, are neglected from the considered reactions. It should be noted the significant presence of H_2O in a reactor is experimentally easy to diagnose and therefore neglecting it in our model is justified. An significant factor to consider when applying this model is temperature or pressure sensitive rate constants such as the desorption of surface hydrogen which is nontrivial in our temperature growth range.[44]

■ ASSOCIATED CONTENT

Supporting Information

Presented are the energy dispersive X-ray spectroscopy for the Ge nanowire structures; additional examples of growths of the discussed morphologies showing high density and consistency. This material is available free of charge via the Internet at http://pubs.acs.org/.

■ AUTHOR INFORMATION

Corresponding Author

*E-mail: spanier@drexel.edu.

Notes

The authors declare no competing financial interest.

■ ACKNOWLEDGMENTS

TEM imaging and analysis were performed in the Drexel Centralized Research Facilities. J.E.S. acknowledges the U.S. Army Research Office for support of this work under W911NF-08-1-0067 and the NSF for instrumentation support under DMR 0722845. C. J. H. was supported by an NSF IGERT Fellowship (DGE 0654313). T. M. was supported by the GAANN-RETAIN program supported by the U. S. Dept. of Education (P200A100117).

■ REFERENCES

(1) Lew, K. K.; Pan, L.; Dickey, E. C.; Redwing, J. M. *Adv. Mater. (Weinheim, Ger.)* **2003**, *15*, 2073−2076.

(2) Kuykendall, T.; Ulrich, P.; Aloni, S.; Yang, P. *Nat. Mater.* **2007**, *6*, 951−956.

(3) Perea, D. E.; Hernesath, E. R.; Schwalbach, E. J.; Lensch-Falk, J. L.; Voorhees, P. W.; Lauhon, L. J. *Nat. Nanotechnol.* **2009**, *4*, 315−319.

(4) Wen, C. Y.; Reuter, M. C.; Bruley, J.; Tersoff, J.; Kodambaka, S.; Stach, E. A.; Ross, F. M. *Science* **2009**, *326*, 1247−1250.

(5) Clark, T. E.; Nimmatoori, P.; Lew, K. K.; Pan, L.; Redwing, J. M.; Dickey, E. C. *Nano Lett.* **2008**, *8*, 1246−1252.

(6) Colli, A.; Fasoli, A.; Beecher, P.; Servati, P.; Pisana, S.; Fu, Y.; Flewitt, A. J.; Milne, W. I.; Robertson, J.; Ducati, C.; De Franceschi, S.; Hofmann, S.; Ferrari, A. C. *J. Appl. Phys.* **2007**, *102*, 034302−1−034302−13.

(7) Dayeh, S. A.; Mack, N. H.; Huang, J. Y.; Picraux, S. T. *Appl. Phys. Lett.* **2011**, *99*, 023102−1−023102−3.

(8) Kolb, F. M.; Berger, A.; Hofmeister, H.; Pippel, E.; Gosele, U.; Zacharias, M. *Appl. Phys. Lett.* **2006**, *89*, 173111−1−173111−3.

(9) Tian, B. Z.; Xie, P.; Kempa, T. J.; Bell, D. C.; Lieber, C. M. *Nat. Nanotechnol.* **2009**, *4*, 824−829.

(10) Wei, D. P.; Chen, Q. *Cryst. Growth Des.* **2010**, *10*, 122−127.

(11) Ross, F. M.; Tersoff, J.; Reuter, M. C. *Phys. Rev. Lett.* **2005**, *95*, No. 146104.

(12) Qian, F.; Li, Y.; Gradecak, S.; Wang, D. L.; Barrelet, C. J.; Lieber, C. M. *Nano Lett.* **2004**, *4*, 1975−1979.

(13) Lauhon, L. J.; Gudiksen, M. S.; Wang, C. L.; Lieber, C. M. *Nature* **2002**, *420*, 57−61.

(14) Doerk, G. S.; Ferralis, N.; Carraro, C.; Maboudian, R. *J. Mater. Chem.* **2008**, *18*, 5376−5381.

(15) Huang, S. L.; Wu, Y.; Zhu, X. F.; Li, L. X.; Wang, Z. G.; Wang, L. Z.; Lu, G. Q. *J. Appl. Phys.* **2011**, *109*, 084328−1−084328−5.

(16) Jeong, M. C.; Oh, B. Y.; Nam, O. H.; Kim, T.; Myoung, J. M. *Nanotechnology* **2006**, *17*, 526−530.

(17) Kodambaka, S.; Hannon, J. B.; Tromp, R. M.; Ross, F. M. *Nano Lett.* **2006**, *6*, 1292−1296.

(18) Kolb, F. M.; Hofmeister, H.; Scholz, R.; Zacharias, M.; Gosele, U.; Ma, D. D.; Lee, S. T. *J. Electrochem. Soc.* **2004**, *151*, G472−G475.

(19) Kolb, F. M.; Hofmeister, H.; Zacharias, M.; Gosele, U. *Appl. Phys. A: Mater. Sci. Process* **2005**, *80*, 1405−1408.

(20) Krylyuk, S.; Davydov, A. V.; Levin, I. *ACS Nano* **2011**, *5*, 656−664.

(21) Li, S.; Zhang, X. Z.; Yan, B.; Yu, T. *Nanotechnology* **2009**, *20*, 495604−1−495604−9.

(22) Nagashima, K.; Yanagida, T.; Oka, K.; Tanaka, H.; Kawai, T. *Appl. Phys. Lett.* **2008**, *93*, 153103−1−153103−3.

(23) Wang, N.; Tang, Y. H.; Zhang, Y. F.; Lee, C. S.; Lee, S. T. *Phys. Rev. B* **1998**, *58*, 16024−16026.

(24) Hannon, J. B.; Kodambaka, S.; Ross, F. M.; Tromp, R. M. *Nature* **2006**, *440*, 69−71.

(25) Jin, C. B.; Yang, J. E.; Jo, M. H. *Appl. Phys. Lett.* **2006**, *88*, 193105−1−193105−3.

(26) Cao, L. Y.; Laim, L.; Ni, C. Y.; Nabet, B.; Spanier, J. E. *J. Am. Chem. Soc.* **2005**, *127*, 13782−13783.

(27) Tang, H.; Chang, J. C.; Shan, Y.; Ma, D. D. D.; Lui, T.-Y.; Zapien, J. A.; Lee, C.-S.; Lee, S.-T. *J. Mater. Sci.* **2009**, *44*, 563−571.

(28) Fan, Z.; Kapadia, R.; Leu, P. W.; Zhang, X.; Chueh, Y.-L.; Takei, K.; Yu, K.; Jamshidi, A.; Rathore, A. A.; Ruebusch, D. J.; Wu, M.; Javey, A. *Nano Lett.* **2010**, *10*, 3823−3827.

(29) Klamchuen, A.; Yanagida, T.; Kanai, M.; Nagashima, K.; Oka, K.; Kawai, T.; Suzuki, M.; Hidaka, Y.; Kai, S. *Appl. Phys. Lett.* **2010**, *97*, 073114−1−073114−3.

(30) Shin, D. H.; Kim, S.; Hong, S. H.; Choi, S. H.; Kim, K. J. *Nanotechnology* **2010**, *21*, 045604−1−045604−4.

(31) Mohammad, S. N. *J. Vac. Sci. Technol., B: Microelectron. Process. Phenom.* **2008**, *26*, 1993−2007.
(32) Zhang, R. Q.; Lifshitz, Y.; Lee, S. T. *Adv. Mater. (Weinheim, Ger.)* **2003**, *15*, 635−640.
(33) Liehr, M.; Dana, S. S.; Anderle, M. *J. Vac. Sci. Technol., A* **1992**, *10*, 869−873.
(34) Racanelli, M.; Greve, D. W. *Appl. Phys. Lett.* **1991**, *58*, 2096−2098.
(35) Takahasi, Y.; Ishii, H.; Fujinaga, K. *Appl. Phys. Lett.* **1990**, *57*, 599−601.
(36) Furumura, Y.; Mieno, F.; Nishizawa, T.; Maeda, M. *J. Electrochem. Soc.* **1986**, *133*, 379−383.
(37) Joyce, B. D.; Baldrey, J. A. *Nature* **1962**, *195*, 485−486.
(38) Murota, J.; Nakamura, N.; Kato, M.; Mikoshiba, N.; Ohmi, T. *Appl. Phys. Lett.* **1989**, *54*, 1007−1009.
(39) Yew, T.-R.; Reif, R. *J. Appl. Phys.* **1989**, *65*, 2500−2507.
(40) Claassen, W. A. P.; Bloem, J. *J. Electrochem. Soc.* **1980**, *127*, 194−202.
(41) Bloem, J.; Claassen, W. A. P. *J. Cryst. Growth* **1980**, *49*, 435−444.
(42) Rathman, D. D.; Silversmith, D. J.; Burns, J. A. *J. Electrochem. Soc.* **1982**, *129*, 2303−2306.
(43) Owen, J. H. G.; Miki, K.; Bowler, D. R.; Briggs, G.; Goldfarb, I. In *Surface Diffusion: Atomistic and Collective Processes*; Tringides, C., Ed.; Plenum Press: New York, 1997.
(44) Lee, J. Y.; Maeng, J. Y.; Kim, A.; Cho, Y. E.; Kim, S. *J. Chem. Phys.* **2003**, *118*, 1929−1936.